Published in final edited form as:
J Neurooncol. 2012 August ; 109(1): 105–114. doi:10.1007/s11060-012-0872-x.

Dual contrast perfusion MRI in a single imaging session for assessment of pediatric brain tumors

Eric M. Thompson,
Department of Neurological Surgery, Oregon Health & Science University, 3303 SW Bond Avenue, CH8N, Portland, Oregon, 97239

Daniel J. Guillaume,
Department of Neurological Surgery, Oregon Health & Science University, 3303 SW Bond Avenue, CH8N, Portland, Oregon, 97239

Edit Dósa,
Department of Neurology, Oregon Health & Science University, 3181 S.W. Sam Jackson Park Road, L603, Portland, Oregon, 97239

Xin Li,
W.M. Keck Foundation High-Field MRI Laboratory–Advanced Imaging Research Center, Oregon Health & Science University, 3181 SW Sam Jackson Park Rd, L452 Portland, OR 97239

Kellie J. Nazemi,
Department of Pediatrics, Division of Hematology and Oncology, Oregon Health & Science University, 3181 S.W. Sam Jackson Park Road CDRC-P, Portland, Oregon, 97239

Seymur Gahramanov,
Department of Neurology, Oregon Health & Science University, 3181 S.W. Sam Jackson Park Road, L603, Portland, Oregon, 97239

Bronwyn E. Hamilton, and
Department of Radiology, Oregon Health & Science University, 3181 SW Sam Jackson Park Rd, CR135, Portland, Oregon, 97239

Edward A. Neuwelt
Department of Neurological Surgery, Oregon Health & Science University, 3303 SW Bond Avenue, CH8N, Portland, Oregon, 97239. Department of Neurology, Oregon Health & Science University, 3181 S.W. Sam Jackson Park Road, L603, Portland, Oregon, 97239. Portland Veterans Affairs Medical Center, 3710 SW US Veterans Hosp. Rd. Portland, Oregon, 97239

Abstract

Ferumoxytol, an iron nanoparticle used as an intravascular contrast agent for perfusion magnetic resonance imaging (MRI), has never been explored the pediatric population. The purpose of this prospective study is to characterize the vascular and permeability properties of pediatric brain tumors using two contrast agents during a single imaging session: ferumoxytol for dynamic susceptibility weighted contrast (DSC) MRI and gadoteridol for dynamic contrast enhanced

Corresponding author: Edward A. Neuwelt, M.D., Department of Neurology, Blood-Brain Barrier Program, Oregon Health & Science University, 3181 Sam Jackson Parkway Road, L603, Portland, OR 97239, Phone: 503-494-7179, Fax: 503-494-5627, neuwelte@ohsu.edu.

Ethical Standard

The aforementioned methods were approved and comply with the Oregon Health & Science Institutional Review Board.

Conflict of Interest

The authors have no conflicts of interest.

(DCE) MRI. In a single imaging session, patients received intravenous ferumoxytol for DSC MRI followed by gadolinium for DCE MRI. Relative cerebral blood volume (rCBV), relative cerebral blood flow (rCBF), transfer coefficient (K^{trans}), and extravascular extracellular space volume fraction (v_e) of the brain lesions were calculated. Patients underwent serial imaging sessions over the course of two years. Of the seven patients enrolled thus far, none has experienced an adverse event. Two patients with medulloblastoma were enrolled preoperatively. In the first, $rCBV_{max}$, rCBF, K^{trans} max, and v_e max values were 3.74, 3.12, 0.47 min^{-1}, and 0.08, respectively, while in the second patient, $rCBV_{max}$, rCBF, K^{trans} max, and v_e max values were 4.72, 3.47, 0.60 min^{-1}, and 0.05, respectively. Four patients were enrolled after new gadolinium enhancement was noted in the tumor resection cavity. In 80% of these lesions, rCBV was < 1 suggestive of pseudoprogression secondary to radiochemotherapy. These preliminary results demonstrate that use of ferumoxytol and gadoteridol contrast agents during a single imaging session is feasible, safe, and appears useful for assessing tumor perfusion and permeability characteristics in children.

Keywords

DSC MRI; DCE MRI; ferumoxytol; brain tumor; pediatric

Introduction

Current magnetic resonance imaging (MRI) that relies upon gadolinium based contrast agents (GBCA) to evaluate brain tumors in children is frequently confounded by false positive results from post-surgical changes and pseudoprogression [1, 2] following radiochemotherapy. Imaging that more accurately predicts the true extent and viability of pediatric brain tumors is of paramount importance, particularly when the imaging can be completed in one session thereby alleviating the need for repeated sedation.

Ferumoxytol is an ultrasmall superparamagnetic iron oxide (USPIO) nanoparticle, with an FDA orphan designation for use as an MRI contrast agent in brain tumor imaging [3]. This agent has demonstrated excellent perfusion brain tumor imaging in adults [4, 5]. The use of ferumoxytol in a pediatric population has never been reported.

Dynamic susceptibility contrast (DSC) MRI allows for the determination of relative cerebral blood flow (rCBF) and relative cerebral blood volume (rCBV) in brain tumors. Because it remains intravascular at early time points [6], ferumoxytol is likely a more accurate marker than GBCA for determining active tumor [7, 8]. Dynamic contrast enhanced (DCE) MRI allows for the determination of the permeability, or “leakiness,” of tumor vasculature such as transfer coefficient (K^{trans}) and extravascular extracellular space volume fraction (v_e). In normal brain with an intact blood brain barrier (BBB), $K^{trans} \approx 0$ min^{-1} [9, 10] and v_e is unmeasurable [11]. Obtaining DSC and DCE MRI in a single imaging session has not been previously reported using both ferumoxytol and GBCA.

An increasingly important problem in pediatric brain tumor imaging is pseudoprogression, an inflammatory brain reaction caused by radiochemotherapy. Our group’s findings suggest that pseudoprogression in adults can be differentiated from true tumor progression more accurately using ferumoxytol-based rather than GBCA-based rCBV measurements with a cut-off ratio of 1.75 [7, 8]. Since patients with pseudoprogression usually recover or stabilize spontaneously without treatment [12], an accurate non-invasive diagnostic method is desirable to avoid unnecessary surgical intervention. The purpose of this prospective study is to more accurately characterize tumor vascular and permeability properties and distinguish true tumor progression from pseudoprogression in pediatric brain tumors using ferumoxytol-based DSC MRI combined with GBCA-based DCE MRI in a single session.

Materials and Methods

This prospective study was approved by the Oregon Health & Science University (OHSU) Institutional Review Board. Consent to be enrolled in this study was obtained from the patient (if applicable) and two parents or legal guardians. Patients included in the study were age 18 years or younger and demonstrated an established histologic diagnosis of a brain tumor.

Study Design

Based on prior studies [5, 7], the starting dose in this study was ≤2 mg Fe/kg to acquire the best imaging results at the applied field strength. The protocol required removal from the study if subjects developed any grade ≥ 3 toxicities from ferumoxytol as defined by the Common Terminology Criteria for Adverse Events v3.0 (CTCAE) [13]. As necessary, monitored anesthesia care and sedation were provided by the OHSU Department of Pediatric Anesthesia. Each patient had a baseline MRI study with any GBCA within 6 weeks prior to enrollment. Laboratory testing included creatinine, calculated GFR, and β-HCG (in females of child bearing potential) within 3 weeks prior each MRI session. Neurological examinations were performed and vital signs were monitored before and after each MRI session.

MRI Acquisition Parameters

All MRI scans were performed on 3T whole-body MRI systems (either TIM Trio, Siemens Medical Solutions, Erlangen, Germany or Achieva, Philips Healthcare, Best, The Netherlands) with a body radio frequency (RF) coil for transmitting and a 12-channel phased array head (Siemens) or an 8-channel sensitivity-encoding head (Philips) coil for signal receiving.

For T_1-weighted spin echo (SE) images, a repetition time (TR)/echo time (TE) of 900/10 was used, and up to 44 slices with a 2-mm thickness without gap were obtained. A field of view (FOV) of 240 × 240 mm and an acquisition matrix of 256 × 256 were chosen. For T_2-weighted turbo spin echo (TSE) images, a TR/TE of 9000/93 was used at a slice thickness of 2 mm without gap. The TSE factor was 9, while the FOV was 240 × 240 mm with an acquisition matrix of 256 × 256. For DSC MRI, dynamic T_2*-weighted images were acquired using a gradient-echo echo-planar imaging pulse sequence (TR, 1500 ms; TE, 20 ms; flip angle (FA), 45°; FOV, 192 × 192 mm; matrix, 64 × 64; and 27 interleaved slices with 3-mm thickness and 0.9-mm gap). After an initial baseline period of 7 series of 27 image slices (11 s), a rapid bolus of ferumoxytol was administered intravenously at a rate of 3 mL/s; followed immediately by 20 mL of saline flush at the same rate. DSC data collection continued for an additional 90 series. DCE MRI employs a 3D fast gradient recalled echo sequence (TR, 5.4–5.8 ms; FA, 15°; FOV, 240 × 180 mm^2; matrix, 256 × 192; 16 or 32 slices; and 96 to 108 DCE time points). 0.1 mmol/kg GBCA was administered approximately 1 minute after commencement of DCE MRI. Multiple FA data for pre-GBCA T_1 estimation was not collected in order to minimize time of pediatric sedation.

Image Analysis

All first-pass DSC MRI data were processed using Lupe (Lund, Sweden) perfusion software. The arterial input function (AIF) was determined from the middle cerebral artery contralateral to the enhancing lesion. Relative CBV measurements were calculated from regions of interest (ROI) that were placed in regions of highest perfusion seen on the rCBV color overlay maps. Four separate ROI measurements were made, and the maximum value ($rCBV_{max}$) was recorded to provide the highest intra- and interobserver reproducibility [14]. The rCBF measurements were taken from areas identical to the region of the $rCBV_{max}$. The

mean of 3 regions of contralateral white matter was used as the internal reference standard. The size of the ROIs was kept constant (radius, 1.5 mm). Parametric maps were analyzed using ImageJ software (NIH, Bethesda, MD, USA).

All DCE MRI data fitting was performed using nonlinear least squares method with an in-house software package written in MATLAB (MathWorks, Natick, MA, USA). A generic AIF derived from previous DCE MRI studies was used for all pharmacokinetic modeling. Standard Toft's model [15] was used for all cases to fit K^{trans} and v_e. Blood volume data was extracted from the DSC MRI using intravascular ferumoxytol. Therefore, blood volume fraction was not modeled in this DCE data because the primary goal of obtaining DCE MRI was to estimate permeability. From pixel by pixel fitting of the entire lesion, heterogenous K^{trans} and v_e values were commonly observed in individual lesions. To standardize lesion characterization, maximum pixel value for each individual lesion was reported for these patients. Dynamic contrast enhancement pharmacokinetic modeling was only applied to areas that contained visible enhancement from post GBCA T_1-weighted images.

Results

From September 2009 to July 2010, 7 patients were enrolled (Table 1). No patient experienced an adverse event secondary to ferumoxytol administration.

Patient 1

Patient 1, a 5 year old male, presented with nausea, vomiting, and ataxia. Conventional MRI showed a midline posterior fossa mass that enhanced homogeneously on post GBCA T_1-weighted MRI. Dynamic MRI showed increased $rCBV_{max}$, rCBF, K^{trans} max, and v_e max (Figure 1, Table 2). The patient underwent gross total resection of the lesion. Intraoperatively, the most vascular areas were encountered in the right posterior aspect of the tumor, consistent with the DSC parametric maps. Additionally, intraoperative ultrasound revealed extraordinarily hyperechoic tumor (images unavailable). Pathology demonstrated medulloblastoma. Routine follow up dynamic MRI 4.5 months post operatively showed substantially decreased $rCBV_{max}$, rCBF, K^{trans} max, and v_e max (Figure 1, Table 2).

Patient 2

Patient 2, a 9 year old female, was enrolled one week following subtotal resection of a medulloblastoma. Post-operative conventional MRI was confounded by artifact from vascular clips and surgical and blood products from the initial resection. Dynamic MRI showed elevated $rCBV_{max}$, rCBF, K^{trans} max, and v_e max (Figure 1, Table 2) in the right posterior aspect of the initial resection cavity in the same area as trace GBCA enhancement on T_1-weighted MRI. The information from the dynamic MRI was used in preoperative planning for a second surgery and in intraoperative localization of the vascular residual tumor thereby facilitating a gross total resection. As in patient 1, intraoperative ultrasound was used to localize the extraordinarily hyperechoic tumor. Intraoperatively, the anterior portion of the previous resection cavity was found to consist primarily of hemostatic agents with minimal residual tumor. These findings were consistent with low vascularity and permeability in this area as demonstrated by dynamic MRI. Gross total resection of the tumor was achieved and conventional MRI 1 year post operatively demonstrated no recurrence.

Patient 3

Patient 3, a 9-year old male, underwent gross total resection of a medulloblastoma one year prior to enrollment. He received adjuvant radiochemotherapy consisting of craniospinal radiation with 54 Gy boost to the posterior fossa in addition to cisplatin, vincristine, and

cyclophosphamide. Nine months following the completion of radiation and 7 months following completion of chemotherapy, a new small linear area of enhancement at the tumor resection cavity was noted on post GBCA T_1-weighted MRI (Figure 1). Despite increased enhancement on post GBCA T_1-weighted MRI, DSC MRI values were < 1.75 (Table 2). This same enhancement and perfusion pattern was reconfirmed 15 weeks later (Figure 1, Table 2). No interventions have been pursued, and the patient remains clinically stable more than a year later.

Patient 4

Patient 4, a 16 year old male, previously underwent gross total resection of a WHO Grade III anaplastic oligoastrocytoma without deletion of chromosomes 1p or 19q. He was treated with adjuvant radiochemotherapy consisting of conformal radiation of 60 Gy and temozolomide. Thirteen months after the completion of radiotherapy, a routine post GBCA T_1-weighted MRI demonstrated a new enhancing nodule in the resection cavity (Figure 2). Dynamic susceptibility weighted contrast MRI values were < 1.75 (Table 2) despite increased post GBCA T_1-weighted MRI suggestive of pseudoprogression. This same pattern in GBCA enhancement and DSC MRI was reconfirmed three months later (Figure 2, Table 2). Dynamic contrast enhancement MRI values were relatively high at both time points likely secondary to differences in the selection of pixels for $rCBV_{max}$ and K^{trans} max. No intervention was pursued and the patient remains clinically stable more than a year later.

Patient 5

Patient 5, a 7-year old male, previously underwent gross total resection of a WHO Grade III anaplastic astrocytoma. Post-operative MRI showed no residual enhancement on post GBCA T_1-weighted MRI. Adjuvant radiochemotherapy consisted of 60 Gy conformal radiation and temozolomide. Nine months following the completion of radiation, post GBCA T_1-weighted MRI demonstrated a new small enhancing nodule in the previous resection cavity (Figure 2). The patient underwent dynamic MRI but these maps could not be interpreted due to the lesion's ROI incorporating the high-flow branches of the anterior cerebral artery.

Patient 6

Patient 6, a 12 year old male, previously underwent near total resection of a right occipital WHO Grade IV glioblastoma multiforme (GBM). He subsequently received 59 Gy conformal radiation and temozolomide followed by concomitant temozolomide and lomustine. Due to vision deterioration, he underwent repeat resection of this lesion with subsequent maintenance temozolomide. Twenty-one months after completing adjuvant radiotherapy and 6 months after stopping temozolomide, an MRI revealed a new focus of enhancement in the medial aspect of the resection cavity and abnormal T_2-weighted signal change in the right cerebellar hemisphere (Figure 3). DSC MRI values of the occipital and cerebellar lesions were < 1.75 (Table 2). The patient died 10 weeks after study enrollment secondary to disease progression of the right cerebellar lesion (Figure 3). The occipital lesion remained stable. A follow-up dynamic MRI session was not obtained secondary to the patient's rapid clinical decline and the family elected not to proceed with an autopsy.

Patient 7

Patient 7, a 7-year-old female, underwent biopsy of a right frontotemporal WHO Grade I juvenile pilocytic astrocytoma (JPA) more than 5 years prior to enrollment. She had been treated with adjuvant carboplatin, vincristine and actinomycin in addition to 3 subsequent tumor debulking surgeries. Dynamic susceptibility contrast MRI values of this avidly

enhancing region were < 1.75 (Figure 3, Table 2), consistent with the historical histological diagnosis of a low-grade glial tumor. Notably, DCE values were relatively high (Table 2).

Discussion

Advanced Imaging Applications

In pediatric medulloblastoma, residual tumor ≥ 1.5 cm^2 places the patients in a "high- risk" category [16] that is associated with worse prognosis [17]. In case 2, the DSC MRI maps demonstrated the true location of residual tumor better than conventional MRI (Figure 1) thereby facilitating a gross total resection. In case 1, post operative dynamic MRI was used to confirm the resection of all tumor areas of high vascularity and permeability.

The use of DSC MRI with ferumoxytol also has important applicability in the evaluation of adjuvant therapy. Differentiating tumor progression from pseudoprogression is critical, as patients often undergo biopsy to help differentiate pseudoprogression from true tumor progression and the presence of pseudoprogression is associated with a more favorable overall survival [18]. The need for advanced imaging assessing perfusion by DSC and permeability by DCE is particularly relevant as these antiangiogenic agents that confound the assessment of tumor progression versus pseudoprogression [19] are being explored in pediatric patients with brain tumors [20, 21].

In our study, patients 3, 4, 5, and 6 were enrolled to evaluate for pseudoprogression. In cases 3, 4, and 6 the lesions in the resection cavity that displayed high degrees of enhancement on post GBCA T_1-weighted MRI exhibited $rCBV_{max}$ suggestive of pseudoprogression. In addition, patients 3 and 4 had stable repeat DSC MRI maps.

The limitation in the determination of pseudoprogression using these methods was seen in Patient 6. Although both DSC and DCE maps did not suggest a highly vascular or permeable lesion in the cerebellum (Table 2), anatomic MRI 6 weeks following the initial dynamic MRI revealed that the lesion had increased in size considerably as seen in both T_2-weighted and post GBCA T_1-weighted MRI (Figure 3). The patient died approximately 4 weeks later. This inaccuracy of these vascular maps was likely due to the incompatibility of the ROI in this study and the size of the enhancing cerebellar lesion. Each ROI in this study had a radius of 1.5 mm while the size of the enhancing lesion was less than 1 mm in diameter. Thus, at least half of the ROI included non-enhancing brain tissue. Based on the results, it is clear that lesions must not only enhance on post GBCA T_1-weighed MRI, but must be greater than the dynamic imaging pixel resolution to minimize partial volume effect in future studies.

Notably, patients' 3, 4, and 6 DCE maps demonstrated relatively high v_e values in the enhancing lesions. The significance of low vascularity and high extravascular extracellular space volume fraction is unknown in this group of patients and warrants further investigation. In patient 7, there was a marked dichotomy in low DSC values and high DCE values. Notably, this was the only patient with a low-grade glioma in this study. This suggests that BBB compromise resulting in increased permeability occurs earlier than increased vascularity in low-grade tumors but not in high-grade tumors.

The results of the DCE MRI values in this study were variable. Variability of permeability within a tumor and between tumors within an individual have been well- documented in both humans [22, 23] and in animal models [24]. The wider K^{trans} and v_e parameter range from DCE MRI may be an indicator of the heterogeneity of tumor growth. Single-pixel hot spots (median K^{trans} ≈0.16 min^{-1}, median v_e ≈0.17) reported for the group is within the range seen in the literature [11, 25, 26]. Still, DSC MRI using ferumoxytol appears to be

more clinically relevant as rCBV has been shown to be the best predictor of tumor grade followed by CBF, and K^{trans} [27]. Future studies will focus on different methods of DCE MRI acquisition and data processing to elucidate how BBB and blood tumor barrier permeability are affected by radiation, chemotherapy, and anti-edema agents such as dexamethasone.

Toxicities

In this study, ferumoxytol doses of 0.7 to 3 mg/kg Fe were administered to patients without adverse events. In our experience in adults, ferumoxytol doses of 1–2 mg/kg Fe provide optimal dynamic imaging quality [5, 7] and are substantially smaller than the dose of 510 mg Fe administered to adults with ESRD to treat anemia [28].

Limitations

The key limitations of this pilot study are the relatively small number of patients, short follow up, and heterogeneous tumor type. Additionally, in order to meet inclusion criteria, the pre-enrollment brain lesion must have enhanced on post GBCA T_1-weighted MRI to allow for the calculation of K^{trans}. Importantly, we also discovered GBCA enhancing lesions must have a radius greater than 1.5 mm and small lesions near large vessels cannot be evaluated using the aforementioned dynamic MRI techniques. This issue may be due to our DSC MRI FOV of 192 × 192 mm which was selected because it had been used by our group in several prior adult dynamic MRI studies [4, 7, 8, 29]. In future DSC and DCE MRI studies in children, we plan on utilizing smaller FOVs.

Although low rCBV in the face of increased post GBCA T_1-weighted MRI is suggestive of pseudoprogression [7], we did not have the opportunity to confirm this by histology in patients 3, 4, and 6. In the case of Patient 2, the effect of artifact from surgical hemostatic agents and metallic vessel clips is unknown in dynamic MRI but certainly has the potential to confound DSC and DCE data. All living patients will continue to be followed with serial dynamic MRI to evaluate change in size or character of their enhancing lesions.

Conclusion

This is the first reported use of ferumoxytol in pediatric patients with brain tumors and the first reported successful dual-contrast single imaging session utilizing ferumoxytol-based DSC and GBCA-based DCE MRI. All patients tolerated ferumoxytol without adverse events in doses of up to 3 mg/kg Fe. We found ferumoxytol-based DSC MRI to be a useful tool preoperatively in devising a tumor resection plan, intraoperatively in localizing the tumor and the most vascular regions of the tumor using ultrasound, and postoperatively in the evaluation of true tumor progression versus pseudoprogression. Dynamic contrast enhanced MRI modeled with the Tofts model was of limited clinical use in our relatively small study group likely secondary to the permeability heterogeneity of each lesion. Based on the pilot data from this study, future studies will be designed using ferumoxytol DSC MRI to focus on the evaluation of pseudoprogression.

Acknowledgments

The authors wish to thank Andy Reikto, M.S. for assistance with the figures. Funding: National Cancer Institute at the National Institutes of Health (CA137488-15S1 American Recovery and Reinvestment Act supplement to E.A.N.).

References

1. Haas-Kogan DA, Banerjee A, Poussaint TY, Kocak M, Prados MD, Geyer JR, Fouladi M, Broniscer A, Minturn JE, Pollack IF, Packer RJ, Boyett JM, Kun LE. Phase II trial of tipifarnib and radiation in children with newly diagnosed diffuse intrinsic pontine gliomas. Neuro Oncol. 2011; 13:298–306. noq202 [pii]. 10.1093/neuonc/noq202 [PubMed: 21339191]
2. Meyzer C, Dhermain F, Ducreux D, Habrand JL, Varlet P, Sainte-Rose C, Dufour C, Grill J. A case report of pseudoprogression followed by complete remission after proton-beam irradiation for a low-grade glioma in a teenager: the value of dynamic contrast-enhanced MRI. Radiat Oncol. 2010; 5:9. 1748-717X-5-9 [pii]. 10.1186/1748-717X-5-9 [PubMed: 20132555]
3. U.S. Food and Drug Administration. [Accessed May 17, 2011] FDA Application: Ferumoxytol. Available at http://wwwaccessdatafdagov/scripts/opdlisting/oopd/OOPD_Results_2cfm?Index_Number=338-411
4. Dosa E, Guillaume DJ, Haluska M, Lacy CA, Hamilton BE, Njus JM, Rooney WD, Kraemer DF, Muldoon LL, Neuwelt EA. Magnetic resonance imaging of intracranial tumors: intra-patient comparison of gadoteridol and ferumoxytol. Neuro Oncol. 2011; 13:251–260. noq172 [pii]. 10.1093/neuonc/noq172 [PubMed: 21163809]
5. Neuwelt EA, Varallyay CG, Manninger S, Solymosi D, Haluska M, Hunt MA, Nesbit G, Stevens A, Jerosch-Herold M, Jacobs PM, Hoffman JM. The potential of ferumoxytol nanoparticle magnetic resonance imaging, perfusion, and angiography in central nervous system malignancy: a pilot study. Neurosurgery. 2007; 60:601–611. discussion 611–602. [PubMed: 17415196]
6. Varallyay CG, Muldoon LL, Gahramanov S, Wu YJ, Goodman JA, Li X, Pike MM, Neuwelt EA. Dynamic MRI using iron oxide nanoparticles to assess early vascular effects of antiangiogenic versus corticosteroid treatment in a glioma model. J Cereb Blood Flow Metab. 2009; 29:853–860. jcbfm2008162 [pii]. 10.1038/jcbfm.2008.162 [PubMed: 19142191]
7. Gahramanov S, Raslan AM, Muldoon LL, Hamilton BE, Rooney WD, Varallyay CG, Njus JM, Haluska M, Neuwelt EA. Potential for differentiation of pseudoprogression from true tumor progression with dynamic susceptibility-weighted contrast-enhanced magnetic resonance imaging using ferumoxytol vs. gadoteridol: a pilot study. Int J Radiat Oncol Biol Phys. 2011; 79:514–523. S0360-3016(09)03560-3 [pii]. 10.1016/j.ijrobp.2009.10.072 [PubMed: 20395065]
8. Gahramanov S, Muldoon LL, Li X, Neuwelt EA. Improved Perfusion MR Imaging Assessment of Intracerebral Tumor Blood Volume and Antiangiogenic Therapy Efficacy in a Rat Model with Ferumoxytol. Radiology. Epub ahead of print. radiol.11103503 [pii]. 10.1148/radiol.11103503
9. Haroon HA, Buckley DL, Patankar TA, Dow GR, Rutherford SA, Baleriaux D, Jackson A. A comparison of Ktrans measurements obtained with conventional and first pass pharmacokinetic models in human gliomas. J Magn Reson Imaging. 2004; 19:527–536.10.1002/jmri.20045 [PubMed: 15112301]
10. Patankar TF, Haroon HA, Mills SJ, Baleriaux D, Buckley DL, Parker GJ, Jackson A. Is volume transfer coefficient (K(trans)) related to histologic grade in human gliomas? AJNR Am J Neuroradiol. 2005; 26:2455–2465. 26/10/2455 [pii]. [PubMed: 16286385]
11. Mills SJ, Soh C, Rose CJ, Cheung S, Zhao S, Parker GJ, Jackson A. Candidate biomarkers of extravascular extracellular space: a direct comparison of apparent diffusion coefficient and dynamic contrast-enhanced MR imaging--derived measurement of the volume of the extravascular extracellular space in glioblastoma multiforme. AJNR Am J Neuroradiol. 2010; 31:549–553. ajnr.A1844 [pii]. 10.3174/ajnr.A1844 [PubMed: 19850765]
12. Brandsma D, Stalpers L, Taal W, Sminia P, van den Bent MJ. Clinical features, mechanisms, and management of pseudoprogression in malignant gliomas. The lancet oncology. 2008; 9:453–461.10.1016/S1470-2045(08)70125-6 [PubMed: 18452856]
13. CTEP. Common Terminology Criteria for Adverse Events v3.0 (CTCAE). 2006.
14. Wetzel SG, Cha S, Johnson G, Lee P, Law M, Kasow DL, Pierce SD, Xue X. Relative cerebral blood volume measurements in intracranial mass lesions: interobserver and intraobserver reproducibility study. Radiology. 2002; 224:797–803. [PubMed: 12202717]
15. Tofts PS, Brix G, Buckley DL, Evelhoch JL, Henderson E, Knopp MV, Larsson HB, Lee TY, Mayr NA, Parker GJ, Port RE, Taylor J, Weisskoff RM. Estimating kinetic parameters from dynamic contrast-enhanced T(1)-weighted MRI of a diffusable tracer: standardized quantities and

symbols. J Magn Reson Imaging. 1999; 10:223–232. [pii]. 10.1002/(SICI)1522-2586(199909)10:3<223::AID-JMRI2>3.0.CO;2-S [PubMed: 10508281]

16. Evans AE, Jenkin RD, Sposto R, Ortega JA, Wilson CB, Wara W, Ertel IJ, Kramer S, Chang CH, Leikin SL, et al. The treatment of medulloblastoma. Results of a prospective randomized trial of radiation therapy with and without CCNU, vincristine, and prednisone. J Neurosurg. 1990; 72:572–582.10.3171/jns.1990.72.4.0572 [PubMed: 2319316]
17. Gilbertson RJ. Medulloblastoma: signalling a change in treatment. Lancet Oncol. 2004; 5:209–218. S147020450401424X [pii]. 10.1016/S1470-2045(04)01424-X [PubMed: 15050952]
18. Brandes AA, Franceschi E, Tosoni A, Blatt V, Pession A, Tallini G, Bertorelle R, Bartolini S, Calbucci F, Andreoli A, Frezza G, Leonardi M, Spagnolli F, Ermani M. MGMT promoter methylation status can predict the incidence and outcome of pseudoprogression after concomitant radiochemotherapy in newly diagnosed glioblastoma patients. J Clin Oncol. 2008; 26:2192–2197. 26/13/2192 [pii]. 10.1200/JCO.2007.14.8163 [PubMed: 18445844]
19. Weinstein JS, Varallyay CG, Dosa E, Gahramanov S, Hamilton B, Rooney WD, Muldoon LL, Neuwelt EA. Superparamagnetic iron oxide nanoparticles: diagnostic magnetic resonance imaging and potential therapeutic applications in neurooncology and central nervous system inflammatory pathologies, a review. Journal of cerebral blood flow and metabolism: official journal of the International Society of Cerebral Blood Flow and Metabolism. 2010; 30:15–35.10.1038/jcbfm.2009.192 [PubMed: 19756021]
20. Benesch M, Windelberg M, Sauseng W, Witt V, Fleischhack G, Lackner H, Gadner H, Bode U, Urban C. Compassionate use of bevacizumab (Avastin) in children and young adults with refractory or recurrent solid tumors. Ann Oncol. 2008; 19:807–813.10.1093/annonc/mdm510 [PubMed: 18056650]
21. Liu AK, Macy ME, Foreman NK. Bevacizumab as therapy for radiation necrosis in four children with pontine gliomas. Int J Radiat Oncol Biol Phys. 2009; 75:1148–1154.10.1016/j.ijrobp.2008.12.032 [PubMed: 19857784]
22. Cha S, Yang L, Johnson G, Lai A, Chen MH, Tihan T, Wendland M, Dillon WP. Comparison of microvascular permeability measurements, K(trans), determined with conventional steady-state T1-weighted and first-pass T2*-weighted MR imaging methods in gliomas and meningiomas. AJNR Am J Neuroradiol. 2006; 27:409–417. [PubMed: 16484420]
23. Mills SJ, Patankar TA, Haroon HA, Baleriaux D, Swindell R, Jackson A. Do cerebral blood volume and contrast transfer coefficient predict prognosis in human glioma? AJNR Am J Neuroradiol. 2006; 27:853–858. 27/4/853 [pii]. [PubMed: 16611778]
24. Lockman PR, Mittapalli RK, Taskar KS, Rudraraju V, Gril B, Bohn KA, Adkins CE, Roberts A, Thorsheim HR, Gaasch JA, Huang S, Palmieri D, Steeg PS, Smith QR. Heterogeneous blood-tumor barrier permeability determines drug efficacy in experimental brain metastases of breast cancer. Clinical cancer research: an official journal of the American Association for Cancer Research. 2010; 16:5664–5678.10.1158/1078-0432.CCR-10-1564 [PubMed: 20829328]
25. Harrer JU, Parker GJ, Haroon HA, Buckley DL, Embelton K, Roberts C, Baleriaux D, Jackson A. Comparative study of methods for determining vascular permeability and blood volume in human gliomas. J Magn Reson Imaging. 2004; 20:748–757.10.1002/jmri.20182 [PubMed: 15503330]
26. Ferl GZ, Xu L, Friesenhahn M, Bernstein LJ, Barboriak DP, Port RE. An automated method for nonparametric kinetic analysis of clinical DCE-MRI data: application to glioblastoma treated with bevacizumab. Magn Reson Med. 2010; 63:1366–1375.10.1002/mrm.22335 [PubMed: 20432307]
27. Law M, Young R, Babb J, Rad M, Sasaki T, Zagzag D, Johnson G. Comparing perfusion metrics obtained from a single compartment versus pharmacokinetic modeling methods using dynamic susceptibility contrast-enhanced perfusion MR imaging with glioma grade. AJNR Am J Neuroradiol. 2006; 27:1975–1982. 27/9/1975 [pii]. [PubMed: 17032878]
28. Lu M, Cohen MH, Rieves D, Pazdur R. FDA report: Ferumoxytol for intravenous iron therapy in adult patients with chronic kidney disease. American journal of hematology. 2010; 85:315–319.10.1002/ajh.21656 [PubMed: 20201089]
29. Hamilton BE, Nesbit GM, Dosa E, Gahramanov S, Rooney B, Nesbit EG, Raines J, Neuwelt EA. Comparative analysis of ferumoxytol and gadoteridol enhancement using T1- and T2-weighted MRI in neuroimaging. AJR Am J Roentgenol. 2011; 197:981–988. 197/4/981 [pii]. 10.2214/AJR.10.5992 [PubMed: 21940589]

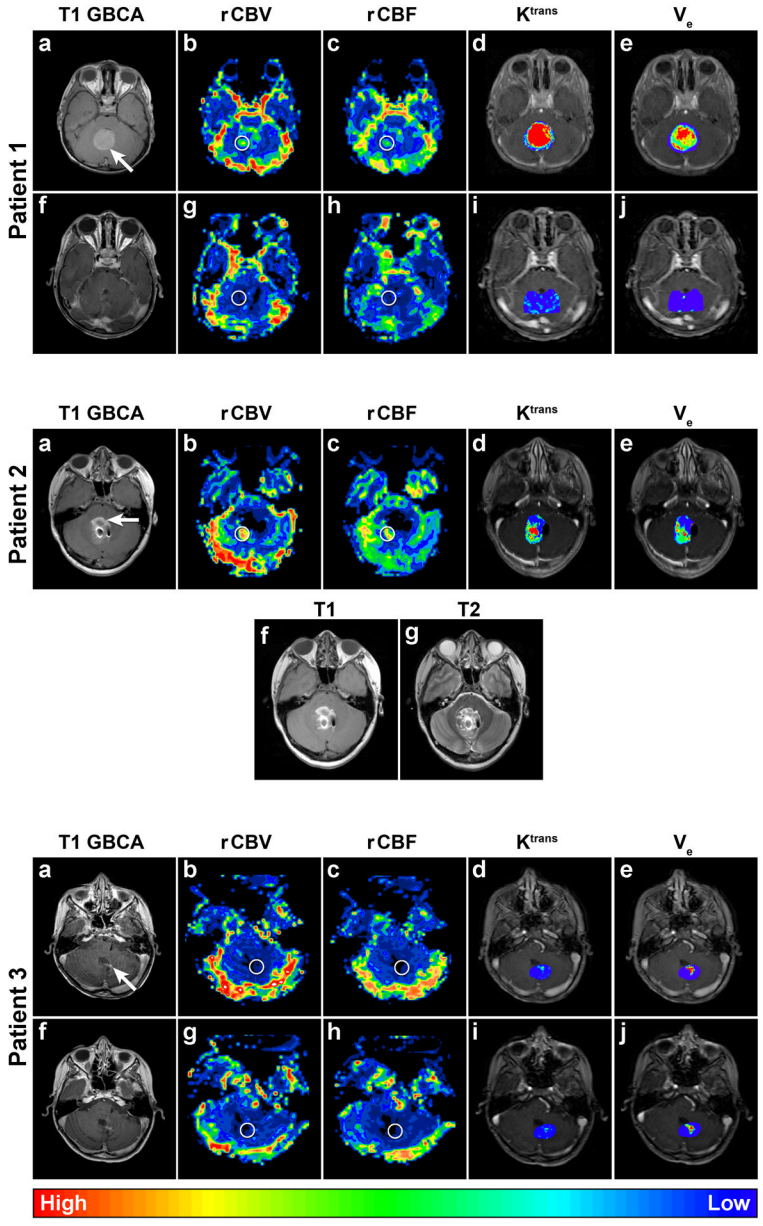

Figure 1.

Patient 1 Axial dynamic MRI parametric maps of Patient 1 with medulloblastoma. Circles indicate region of interest (ROI). The circles in these figures are larger than the actual ROIs for clarity. The top row (a–e) is preoperative images. The conventional post GBCA T_1-weighted MRI (a) shows a homogenously enhancing tumor in the posterior fossa (arrow). DSC MRI parametric maps (b–c) demonstrate elevated vascularity in the tumor: $rCBV_{max}$ = 3.74 and rCBF = 3.12. DCE MRI parametric maps (d–e) demonstrate elevated K^{trans} with a maximum pixel value ≈0.47 min^{-1} and heterogenous v_e with a maximum pixel value ≈0.08. The bottom row (f–j) was obtained postoperatively and demonstrates complete tumor resection and substantially reduced vascularity: $rCBV_{max}$ = 0.69 and rCBF = 0.81, and permeability: K^{trans} max ≈0.03 min^{-1} and v_e max ≈0.01. Of note, choroid plexus of the fourth ventricle was not visible on preoperative images and was not included in the ROI of the postoperative parametric maps.

Patient 2. Axial dynamic MRI parametric maps of Patient 2 with medulloblastoma. Circles indicate ROI. The conventional post GBCA T_1-weighted MRI (a) demonstrates poorly-defined trace enhancement in the right posterior portion of the resection cavity (arrow) when compared to the pre-contrast T_1-weighted image (f). T_2-weighted MRI (g) demonstrated high signal surrounding the entirety of the 4th ventricle and thus was also not particularly helpful in differentiating residual tumor from surgical products and clip artifact. However, dynamic MRI parametric maps (b–e) reveal that the most vascular and permeable component of the residual tumor is in the right posterior aspect: $rCBV_{max}$ = 4.72, rCBF = 3.47, K^{trans} max ≈0.60, and v_e max ≈0.05. The artifact in the resection cavity is due to vascular clips placed during the initial resection. Choroid plexus of the fourth ventricle was not included in the ROI.

Patient 3. Axial dynamic MRI parametric maps of Patient 3 with medulloblastoma. Circles indicate ROI. The top row (a–e) was obtained after a new small area of enhancement was noted in the resection cavity (a, arrow) on post GBCA T_1-weighted MRI. DSC MRI parametric maps (b–c) demonstrate low vascularity: $rCBV_{max}$ = 0.54 and rCBF = 0.80. DCE parametric maps (d–e) demonstrate low K^{trans} max ≈0.05 but relatively high v_e max ≈0.15. The bottom row images (f–j) were obtained 15 weeks after the first dynamic MRI and demonstrate stable post GBCA T_1- weighted MRI (f) and dynamic MRI parametric maps $_{trans}$ (g–j): $rCBV_{max}$ = 0.66, rCBF = 0.66, K max ≈0.04, and v_e max ≈0.24. Findings on both studies and the lack of temporal progression support the diagnosis of pseudoprogression.

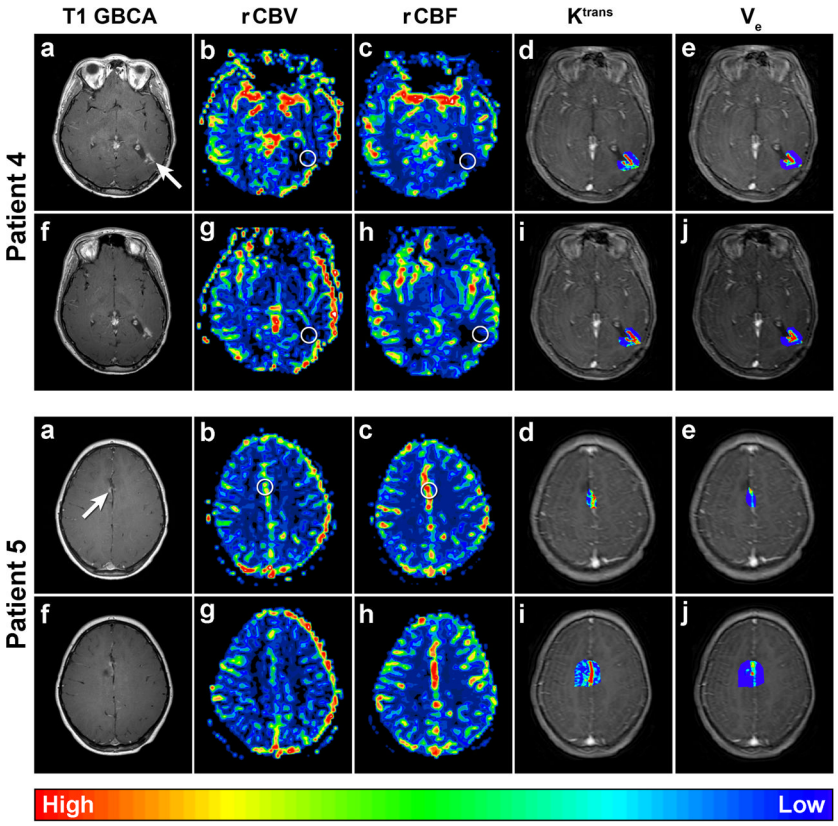

Figure 2.

Patient 4 Axial dynamic MRI parametric maps of Patient 4 with anaplastic oligoastrocytoma. Circles indicate ROI. The top row images were obtained after a new small area of enhancement was noted in the resection cavity (a, arrow) on post GBCA T_1-weighted MRI. DSC MRI parametric maps (b–c) demonstrate low vascularity: $rCBV_{max}$ = 0.85 and rCBF = 0.57, while DCE MRI parametric maps (d–e) demonstrate elevated permeability: K^{trans} max ≈0.23 and v_e max ≈0.18. The bottom row images (f–j) were obtained 3 months after the first DSC MRI and demonstrate minimally increased post GBCA T_1-weighted MRI (f) and dynamic MRI parametric maps (g–j): $rCBV_{max}$ = 0.99, rCBF = 0.90, K^{trans} max ≈0.47, v_e max ≈0.19. Findings on both studies and the lack of substantial temporal progression support pseudoprogression.

Patient 5. Axial dynamic MRI parametric maps of Patient 5 with anaplastic astrocytoma. Circles indicate ROI. The top row images were obtained after a new small area of enhancement was noted in the resection cavity (a, arrow) on post GBCA T_1-weighted MRI. Dynamic MRI parametric maps (b–e) could not be interpreted secondary to the ROI including branches from the anterior cerebral artery. The bottom row images (f–j) were obtained 3 months following the first dynamic MRI and show no obvious change in the post GBCA T_1-weighted, DSC, or DCE MRI.

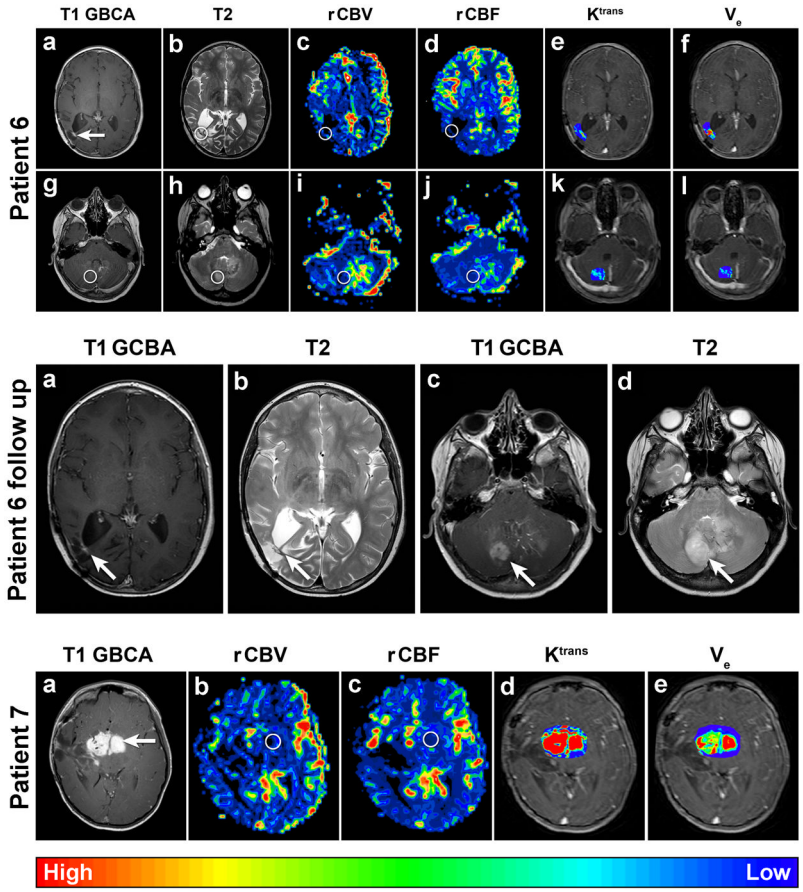

Figure 3.

Patient 6 Axial dynamic MRI parametric maps of Patient 6 with GBM. Circles indicate ROI. All images were obtained after the development of a new enhancing area in the right occipital region resection cavity (a, arrow) on post GBCA T_1-weighted MRI with corresponding increased T_2- weighted signal (b) noted on surveillance MRI. Additionally, a new area of increased T_2- weighted signal in the cerebellum (h, circle) with a sub-millimeter area of enhancement (g) was noted. DSC MRI parametric maps with the ROI on the occipital enhancement (c–d) demonstrate low vascularity: $rCBV_{max}$ = 0.92 and rCBF = 0.64. DCE parametric maps (e–f) demonstrate low K^{trans} max ≈0.08 and relatively high v_e max ≈0.23. DSC MRI parametric maps with the ROI on the cerebellar T_2-weighted hyperintensity (i–j) also demonstrate low vascularity: $rCBV_{max}$ = 0.89 and rCBF = 0.77. DCE MRI parametric maps (k–l) demonstrate low permeability: K^{trans} max ≈0.04 and v_e max ≈0.01. Note that T_2 signal and perfusion asymmetry visible in the left cerebellar hemisphere just posteriolateral to the fourth ventricle was related to the presence of a prominent developmental venous anomaly on conventional images (g).

Patient 6 follow up. Axial T_1-weighted MR images after GBCA administration (a and c) and T_2-weighted MR images (b and d) of Patient 6 obtained 6 weeks after the above dynamic MRI maps. Note the substantial interval increase in size of the right cerebellar lesion (c and d) compared to that seen in the first dynamic maps above (g and h).

Patient 7. Axial dynamic MRI parametric maps of Patient 7 with JPA. Circles indicate ROI. The images were obtained to evaluate this avidly enhancing region (a, arrow) on post GBCA T_1- weighted MRI. DSC MRI parametric maps (b–c) demonstrate vascularity similar to normal control brain parenchyma: $rCBV_{max}$ = 0.96, rCBF = 0.78. However, DCE MRI

parametric maps (d–e) demonstrate increased permeability: K^{trans} max ≈0.45 and v_e max ≈0.27.

Table 1

Patient Characteristics

Patient	Age (years)	Diagnosis	Reason for enrollment	Interval from completion of radiotherapy at enrollment (months)	Fe dose (mg/kg) first dynamic MRI	Fe dose (mg/kg) second dynamic MRI
1	5	Medulloblastoma	Preoperative planning and evaluation of vascularity, postoperative assessment of tumor resection	NA	2	2
2	9	Medulloblastoma	Preoperative planning and determination of residual tumor	NA	2	NA
3	9	Medulloblastoma	Evaluation of tumor progression versus pseudoprogression	9	1	1
4	16	Anaplastic Oligoastrocytoma	Evaluation of tumor progression versus pseudoprogression	13	0.7	0.7
5	7	Anaplastic Astrocytoma	Evaluation of tumor progression versus pseudoprogression	11	1	3
6	12	Glioblastoma Multiforme	Evaluation of tumor progression versus pseudoprogression	21	1	1
7	7	Juvenile Pilocytic Astrocytoma	Evaluation of possible high-grade characteristics tumor	NA	1	NA

Table 2

Dynamic Imaging Results

Patient	Presumptive diagnosis	Scan number	rCBV max	rCBF max	K^{trans} max (min^{-1})	v_e max
1	Medulloblastoma	1	3.74	3.12	0.47	0.08
		2	0.69	0.81	0.03	0.01
2	Residual Medulloblastoma	1	4.72	3.47	0.60	0.05
3	Pseudoprogression	1	0.54	0.80	0.05	0.15
		2	0.66	0.66	0.04	0.24
4	Pseudoprogression	1	0.85	0.57	0.23	0.18
		2	0.99	0.90	0.47	0.19
5	Pseudoprogression	1	Indeterminate			
		2	Indeterminate			
6	Pseudoprogression	1, occipital lesion	0.92	0.64	0.08	0.23
	Tumor progression	1, cerebellar lesion	0.89	0.77	0.04	0.01
7	Recurrent JPA	1	0.96	0.78	0.45	0.27
		Mean	0.93	0.73	0.25	0.14
		Median	0.92	0.77	0.16	0.17

Abbreviations: JPA, Juvenile Pilocytic Astrocytoma